

MATERIALS SCIENCE

Special Topic: Advanced Materials for Solar Energy Conversion

Polar or nonpolar? That is not the question for perovskite solar cells

Boyuan Huang^{1,2}, Zhenghao Liu³, Changwei Wu³, Yuan Zhang³, Jinjin Zhao⁴,
Xiao Wang^{3,*} and Jiangyu Li^{1,2,3,*}

¹Department of Materials Science and Engineering, Southern University of Science and Technology, Shenzhen 518055, China; ²Guangdong Key Laboratory of Functional Oxide Materials and Devices, Southern University of Science and Technology, Shenzhen 518055, China; ³Shenzhen Key Laboratory of Nanobiomechanics, Shenzhen Institute of Advanced Technology, Chinese Academy of Sciences, Shenzhen 518055, China and ⁴School of Materials Science and Engineering, Key Laboratory of Smart Materials and Structures Mechanics of Hebei Province, Shijiazhuang Tiedao University, Shijiazhuang 050043, China

*Corresponding authors. E-mails: xiao.wang@siat.ac.cn; lijy@sustech.edu.cn

Received 29

December 2020;

Revised 6 May 2021;

Accepted 19 May

2021

ABSTRACT

Perovskite solar cells (PSC) are promising next generation photovoltaic technologies, and there is considerable interest in the role of possible polarization of organic-inorganic halide perovskites (OIHPs) in photovoltaic conversion. The polarity of OIHPs is still hotly debated, however. In this review, we examine recent literature on the polarity of OIHPs from both theoretical and experimental points of view, and argue that they can be both polar and nonpolar, depending on composition, processing and environment. Implications of OIHP polarity to photovoltaic conversion are also discussed, and new insights gained through research efforts. In the future, integration of a local scanning probe with global macroscopic measurements *in situ* will provide invaluable microscopic insight into the intriguing macroscopic phenomena, while synchrotron diffractions and scanning transmission electron microscopy on more stable samples may ultimately settle the debate.

Keywords: perovskite solar cells, polarity, ferroelectricity, first-principles calculations, scanning probe, photovoltaic implication

INTRODUCTION

Ever since the spectacular rise of perovskite solar cells (PSCs), there have been suggestions on possible roles of ferroelectric polarization in their photovoltaic conversion. Perovskite materials, particularly oxides, are often ferroelectric, and early theoretical calculations indicated that polarization in organic-inorganic halide perovskites (OIHPs) may help charge separation and facilitate carrier transport [1]. However, the ferroelectricity of OIHPs has not been firmly established experimentally, and the possible polarity of OIHPs is still hotly debated [2,3]. There is considerable theoretical and experimental evidence to support either point of view [4]. Both nonpolar I4/mcm (Fig. 1a) and polar I4cm (Fig. 1b) space groups are possible for CH₃NH₃PbI₃ (MAPI) [5–7], and the structural difference is very subtle, making it difficult to differentiate these by conventional structural characterization techniques such as diffraction. Indeed, the structure details of MAPI have not been fully resolved, and the poor stabil-

ity of the materials exacerbates the problem. In this review, we examine recent literature on the polarity of OIHPs, and argue that they can be both polar and nonpolar, depending on composition, processing and environment. Implications to photovoltaic conversion, especially hysteresis, are also discussed.

THEORETICAL CONSIDERATIONS

Differing from traditional perovskite, the component at the A site in OIHP is positioned by a molecule-type ion, which may have an intrinsic dipole and induce the deformation of the octahedron framework caused by the interatomic hydrogen bond. Therefore, the apparent polarization of OIHP is the collective polarization of each unit impacted by the orientation of the A-site molecule. In the case of MAPI, the major structural difference between the polar I4cm and nonpolar I4/mcm phases is the orientation of MA cations, which have an intrinsic dipole of ~ 2.3 D [1]. In the polar

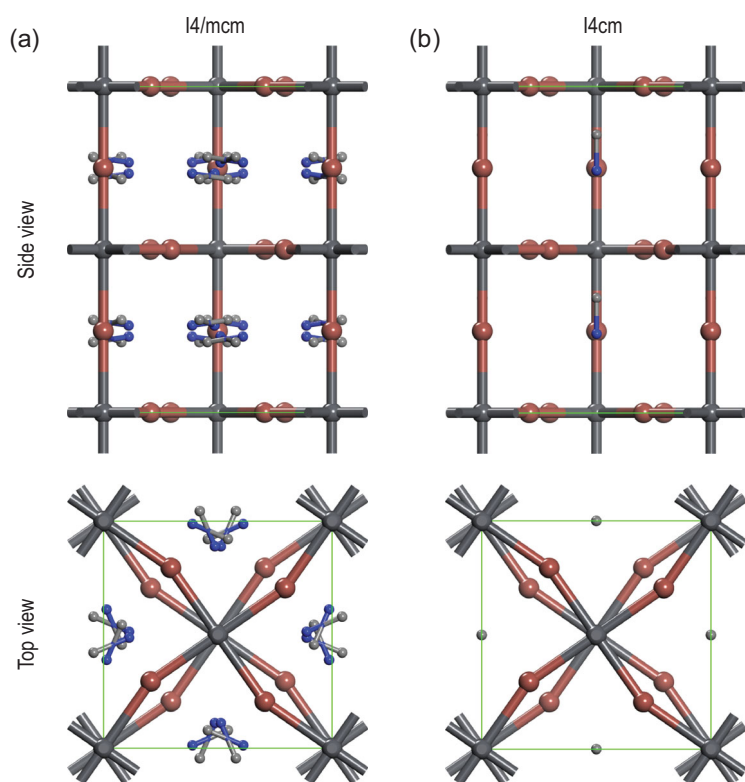


Figure 1. Schematic lattice of nonpolar $I4/mcm$ (a) and polar $I4cm$ (b) space groups for MAPI from side and top views. The hydrogen atoms are hidden for simplicity.

phase, the C–N dipole shows a ‘head-tail’ alignment along the c axis and displays a large polarization of several $\mu\text{C}/\text{cm}^2$ [8–11], whereas in the nonpolar counterpart, because of space group symmetry, each MA cation is usually described with partial occupancies with four identical positions and thus exhibits no net polarization [12]. Nevertheless, the orientation of an MA cation can distort the neighboring iodides from their centrosymmetric positions, leading to ferroelectricity [13].

The optimal orientation of MA in MAPbI_3 bulk has not yet been determined through theoretical models and methods. Brivio *et al.* calculated the total energy of MA arrays along $\langle 100 \rangle$, $\langle 110 \rangle$ and $\langle 111 \rangle$ directions in the cubic phase and found that $\langle 100 \rangle$ is the most stable orientation with energy difference less than 15 meV per atom [14]. Bechtel *et al.* calculated the full energy landscape for rigid-body rotations and translations of MA in the cubic phase and reached the same conclusion. They revealed that the preferential orientation is attributed to the strong N–H...I interactions between MA and the Pb–I framework along the $\langle 100 \rangle$ direction [15]. However, others reached different conclusions. Shimamura *et al.* used a cubic symmetry-assisted analysis and found that the prominent orientation of MA is in crystalline $\langle 110 \rangle$ directions, rather than the $\langle 100 \rangle$ and $\langle 111 \rangle$ di-

rections [16]. Xu *et al.* studied MA orientation using the swarm intelligence-based structure prediction method combined with DFT calculations, but they found that the $\langle 012 \rangle$ orientation was most stable rather than the aforementioned directions [17].

Despite the puzzling optimal orientation, there is agreement that the orientation of MA tunes the strength and direction of the hydrogen bond between MA^+ and I^- , which is rather weak (~ 0.09 eV/cation) [18]; there is only slight energy difference (< 0.1 eV/unit) between the two phases and the phase transition barrier is also quite small (about 0.2 eV/unit) [9]. Such a tiny difference makes for an easy transition between the polar and nonpolar phases at room temperature [19,20]. Furthermore, the subtlety between the two phases also makes the debate regarding polar and nonpolar nature of OIHPs notably dependent on method, model, size and time-scale in ab initio calculations [9,21]. We should not only focus on the origin of the polarity in its primitive cell, but also the long-range dynamics of the MA cations in a wider vision. The ab initio molecular simulation is a versatile method that can consider more operational conditions (such as temperature, long-range dynamics, etc.) with accuracy. The random order of MA and the phase transition between the two phases have been tracked, usually indicating an antiferroelectric nature of tetragonal OIHPs [19,20,22].

As mentioned, the phase transition causes reorientation of the MA cation and changes the hydrogen bond, which is very weak and has little contribution to the valence band maximum (VBM), conduction band minimum (CBM) or even band gap (~ 0.1 eV fluctuation) [23,24] (Fig. 2c). However, the influence of the collective behavior of MA dynamics on the band structure cannot be neglected, as this will influence the photoelectric performance. Geng *et al.* designed several MA orientations in a supercell and tracked the band gap of MAPI. Their theoretical results showed that the band gap is tunable, ranging from 1.3 to 1.6 eV [25]. Mosconi *et al.* performed ab initio molecular dynamics simulations and also found a variation of ± 0.1 to 0.2 eV of the electronic properties with the ion dynamics [22], which is consistent with Mladenović’s works [26]. Besides the value of the band gap, the orientation of MA can also cause transition from direct band gap to indirect band gap. Motta *et al.* performed van der Waals-corrected DFT calculations and revealed that the band gap will become indirect if MA orients along a $\langle 011 \rangle$ -like direction, causing dynamic change of the band structure which might be the origin of the slow carrier recombination of MAPI [27]. Later they found a similar direct–indirect transition

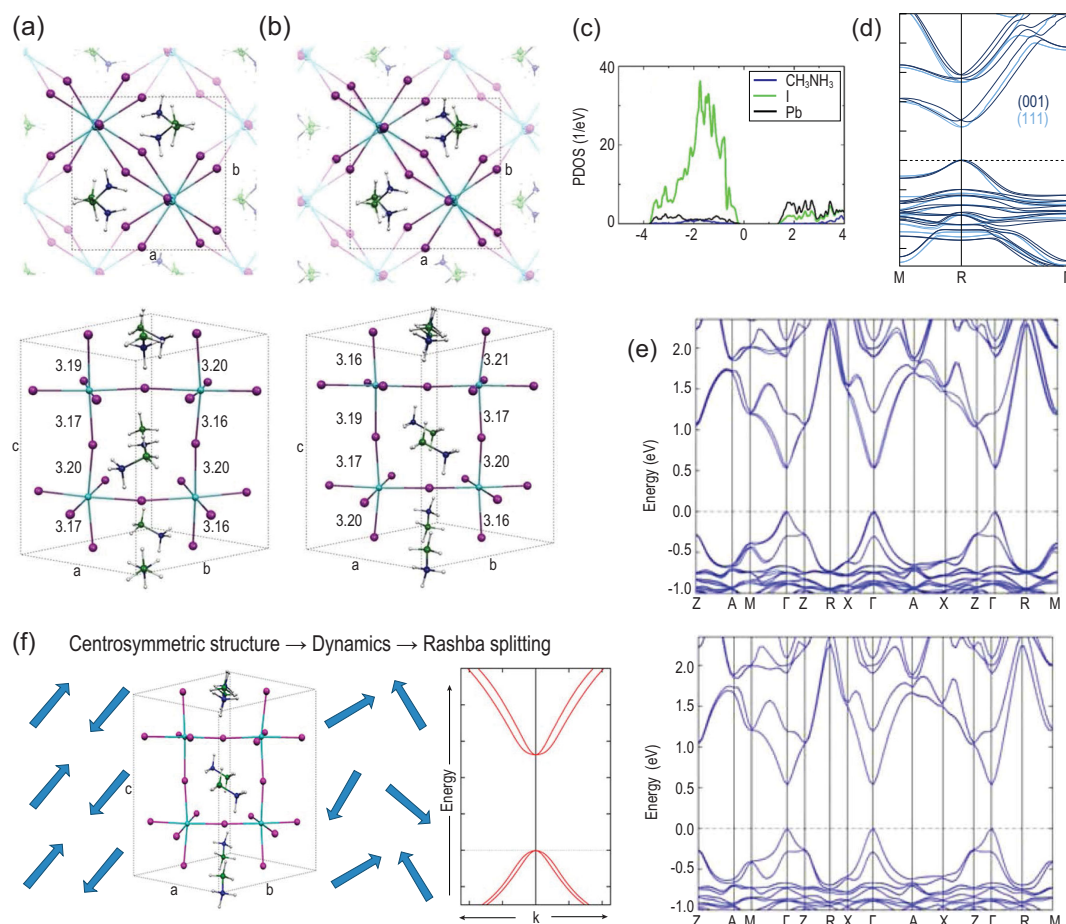


Figure 2. Theoretical studies on photovoltaic properties of polar and nonpolar MAPI in bulk phase. The top and side views of (a) polar and (b) nonpolar phases of MAPI relying on the orientation of MA cation. The Pb, I, C, N, H atoms are colored in light blue, pink, blue, green and white. (c) Projected density of states of MAPI. The Pb and I instead of MA group mainly contribute to the CBM and VBM. (d) Band structure of MAPbBr₃ (MAPB) with MA along different directions. A direct to indirect band transition is present when the orientation of MA changes from $\langle 111 \rangle$ to $\langle 001 \rangle$ direction. (e) The Rashba/Dresselhaus effect in the polar phases. Band splitting is present near the CBM and VBM in the polar phase, while in the nonpolar phase, the Rashba/Dresselhaus effect does not exist. (f) The dynamic Rashba effect in MAPI caused by random rotation of MA. Adapted with permission from Refs [9,24,28,31].

in MAPbBr₃ (MAPB). Their DFT calculations demonstrated that MAPB is a direct band gap semiconductor when MA is oriented along the $\langle 111 \rangle$ direction but turns indirect along the $\langle 100 \rangle$ direction (Fig. 2d) [28].

The Rashba/Dresselhaus effect is a phenomenon in solid-state physics in which spin-orbit interaction causes energy bands to split, especially in a crystal system lacking inversion symmetry. The polar OIHP is a typical case in which to present such effect. In the 14cm polar phase (shown in Fig. 2a), the Rashba effect can be detected by ab initio calculations, resulting in splitting of frontier orbitals near Fermi level along the M-Γ-Z direction and creation of an indirect band gap (Fig. 2e) [9,29], while in the I4/mcm nonpolar phase (Fig. 2b), the Rashba effect does not exist (Fig. 2e) [12]. Niesner *et al.* used angle-resolved photoelectron spectroscopy and de-

tected the Rashba/Dresselhaus effect in MAPB [30], which is consistent with theoretical prediction. Furthermore, a ‘dynamic Rashba effect’ was proposed by Etienne *et al.* through the rotation of MA or the deformation of the framework when the thermal movement of MA was tracked by van der Waals-corrected ab initio simulations (Fig. 2f) [31]. Such an effect might lead to reduced recombination rate caused by a spin-forbidden transition [32]. Niesner *et al.* resonantly excited photocurrents in single-crystalline tetragonal MAPI with circularly polarized light to clarify the existence of such effect. Further studies showed that the energy splitting between the spin-polarized transition and the direct optical transition, as well as the amplitude of the circular photogalvanic effect, increased with temperature [33]. Wu *et al.* used a broad range of temperature-dependent and time-resolved optical

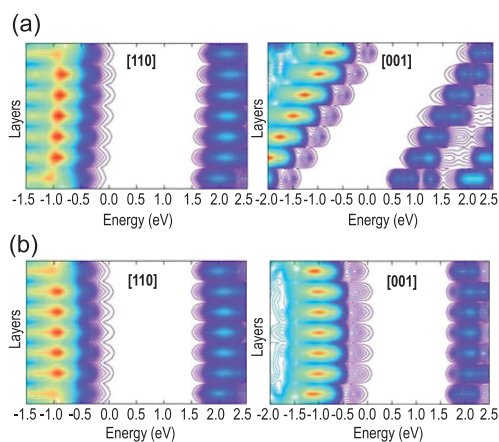


Figure 3. Density of states (DOS) of the valence and conduction bands for the surface constructed from (a) polar and (b) nonpolar phases along [110] and [001] directions. Adapted with permission from Ref. [9].

spectroscopies, correlated with density functional theory (DFT) and molecular dynamics (MD) calculations and electrical characterizations, and proved the existence of indirect tail states below the direct transition edge in MAPB arising from a dynamical Rashba splitting effect [34]. Recalling the general features of Rashba/Dresselhaus splitting, Kepenekian *et al.* used symmetry analysis and DFT

calculations and discussed the possibility of designing spintronic devices. They found even in the centrosymmetric system, the Rashba effect can be present under the external electric field [35]. The polarization can also impact electronic properties of the surface structure apart from the bulk. The orientation of MA cations can give rise to strong bending in the valence and conduction bands of polar phases, as exhibited by a gradient in density of states (DOS) along the [001] direction (Fig. 3a). Such band bending may reduce the carrier recombination and assist charge separation [9]. For the nonpolar phase (Fig. 3b), on the other hand, DOS along both [110] and [001] directions are nearly constant. In the mesoscopic or macroscopic system, the domain wall can be formed in OIHP and display different electronic properties compared with the bulk. Chen *et al.* studied the formation and band gap vs the domain width. As shown in Fig. 4a, they reported that the domain is stable with rather low formation energy and that increasing the domain width can decrease the electronic band gap from ~ 1.4 eV to 0 [36]. The MA orientation can tune the charge aggregation near CBM and VBM [37] (shown in Fig. 4c), which might act as the ‘ferroelectric highway’ and profit the carrier separation [1]. The polarization in ferroelectric domains can suppress the nonradiative electron-hole recombination based on

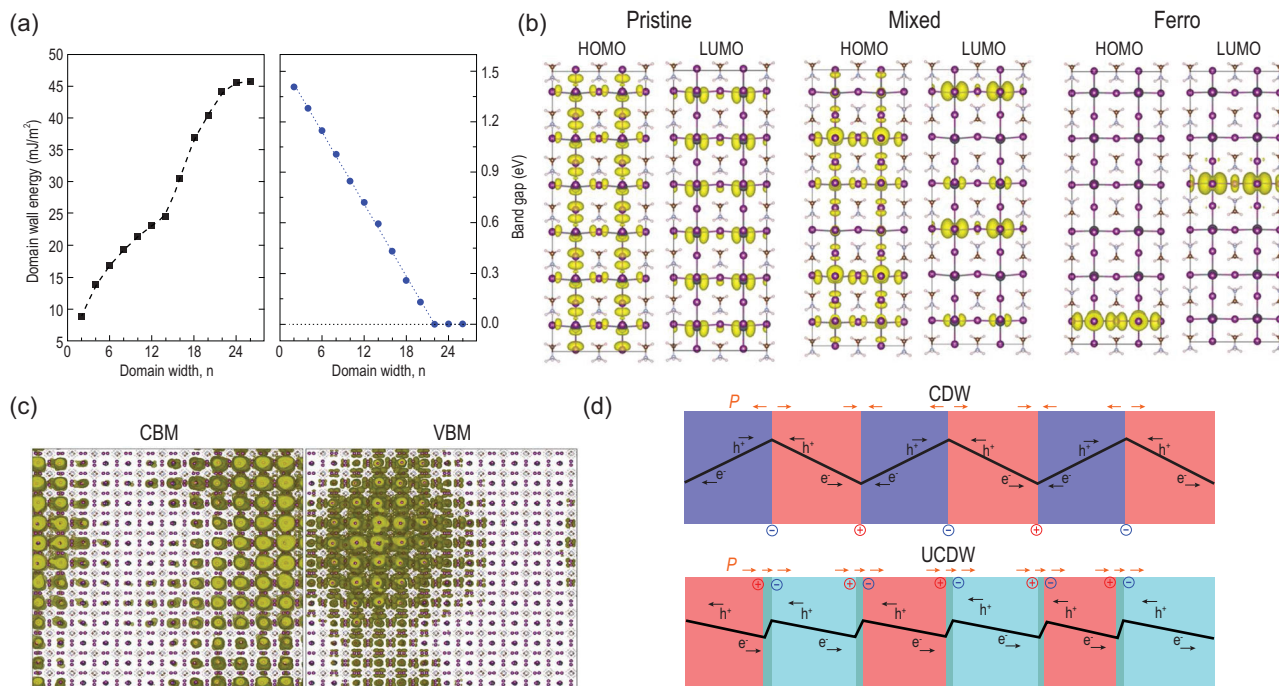


Figure 4. Theoretical studies on the properties of the domain wall in MAPI. (a) Domain wall energy and electronic band gap as a function of domain width in MAPI. (b) The highest occupied molecular orbital (HOMO) and lowest unoccupied molecular orbital (LUMO) charge densities in pristine MAPI, mixed and ferro systems. (c) The charge density of the CBM and VBM states in the MAPI supercell with MA randomly oriented. Both the CBM and VBM charge densities are strongly localized. (d) The charged (top) and uncharged (bottom) domain walls formed by the orientation of MA cation. Head-to-head and tail-to-tail charge domain walls attract electron and hole, respectively, facilitating charge separation. Adapted with permission from Refs [36–39].

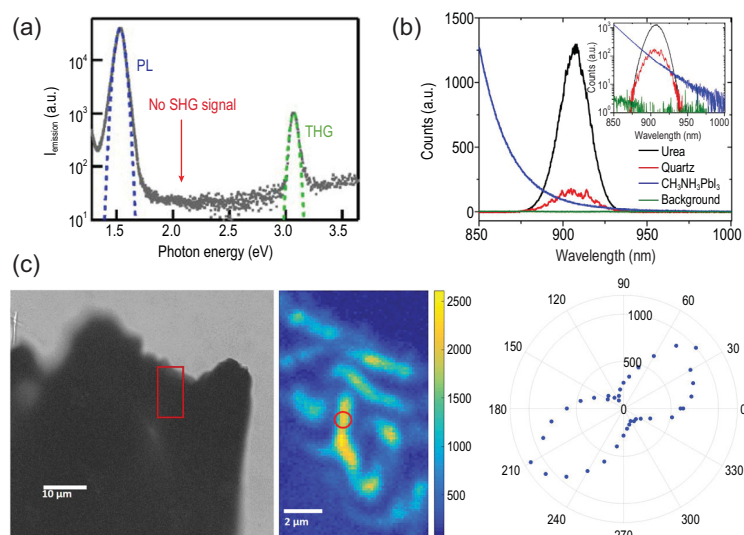


Figure 5. Second harmonic generation (SHG) response. (a) Emission spectra of MAPI under excitation at 1.03 eV. (b) Spectra of second harmonic generated at 900 nm, with incident 1800 nm laser pulse measured on urea (in black) at 1.75 mW incident power, quartz (in red) at 14.9 mW, and MAPI (in blue) at 14.9 mW after subtracting the detector background, which is shown in green. (c) A polar plot of the SHG signal (right) from the marked point in the middle SHG mapping, the area of which is approximately marked by the red box in the bright-field transmission image (left) of a crystal fragment. Adapted with permission from Refs [62,67,76].

the time-domain *ab initio* study (Fig. 4b) [38]. Here, the pristine system is pure I4cm polar phase with aligned C–N bonds, the mixed system refers to a mixture of aligned and anti-aligned C–N bond pairs, presenting nonpolar characteristics, while the ferro-system contains two domains with opposite C–N polar bonds. Charge separation is clearly observed in mixed and ferro-systems with opposite polar axes, beneficial for recombination suppression. Furthermore, when the domain wall is charged, the band gap can be reduced by 20–40%, and there is a strong potential step that facilitates electron-hole separation (Fig. 4d), providing segregated channels for photoexcited charge carriers [39], which are desirable for high conversion efficiency [1]. Summarizing these theoretical studies, there is general agreement that polarization may be beneficial for photovoltaic conversion.

EXPERIMENTAL EVIDENCE

Given the uncertainty associated with two possible tetragonal lattices for MAPI (Fig. 1), it was natural to carry out detailed structure analysis via X-ray and neutron diffraction techniques [40–45]. However, the subtle structural difference has proven difficult to resolve, and the data can be fit by either polar [20,38,46–58] or nonpolar [8,19,59–68]

space groups. Attempts have also been made using transmission electron microscopy (TEM) [69–71], although the materials are prone to degradation [72] and it is virtually impossible to get an atomically resolved image with one exception, wherein an HRTEM image acquired from more stable MAPbBr₃ (MAPB) showed polar domains [73]. As a result, much effort has been devoted to functional probing, as the properties of polar and nonpolar groups are drastically different. Macroscopic ferroelectric, pyroelectric and dielectric measurements have also been carried out [48,50,59,60,64,66,74–76], although leakage current and ionic migration often make the data interpretation ambiguous. While polar structure, with the breaking of inversion symmetry, is expected to be active in optical second harmonic generation (SHG) [12], the experimental data are inconclusive because of the strong background from other nonlinearities [62,77]. Absence of macroscopic SHG was first reported by Yamada *et al.* (Fig. 5a) [67,77], who did not observe any SHG signal under excitation at 1.03 eV (1204 nm) after application of a poling electric field around 1 kV/cm to the sample, while third harmonic generation and PL signals were clear because of two-photon absorption. To exclude the possibility that the second harmonic generated at wavelengths <800 nm would be strongly absorbed by MAPI in view of its small band gap, Govinda *et al.* adopted 1800 nm to perform SHG experiments, but the absence of a SHG response at 900 nm was still evident (Fig. 5b) [62]. It remains possible that ferroelectric domain size is below laser wavelength. Indeed, spatially resolved SHG mapping (Fig. 5c) provided strong evidence on polar domains in MAPI [76], and local polarity can be averaged out at macroscopic scale, which highlights the importance of spatially resolved local probing. Piezoresponse force microscopy (PFM) is a powerful tool to probe local electromechanical coupling at the nanoscale [78,79], and it has been widely applied to study OIHPs. Not surprisingly, PFM data reported largely fall into two categories, supporting either polar [46,47,49–54,56–58] or nonpolar [8,61,63,65,68,80] structure. In fact, even with quite similar experimental observations, for example characteristic lamellar domain patterns reported by different groups [53,81], the interpretations can be completely opposite. This is because electromechanical responses as probed by PFM can arise from complex microscopic mechanisms [82], especially ionic activities, making PFM data analysis for OIHPs nontrivial. This is best illustrated by the recent debates in *Nature Materials* [2,3] on the chemical nature of ferroelastic domains in MAPI reported by Liu *et al.* [68], and there is no

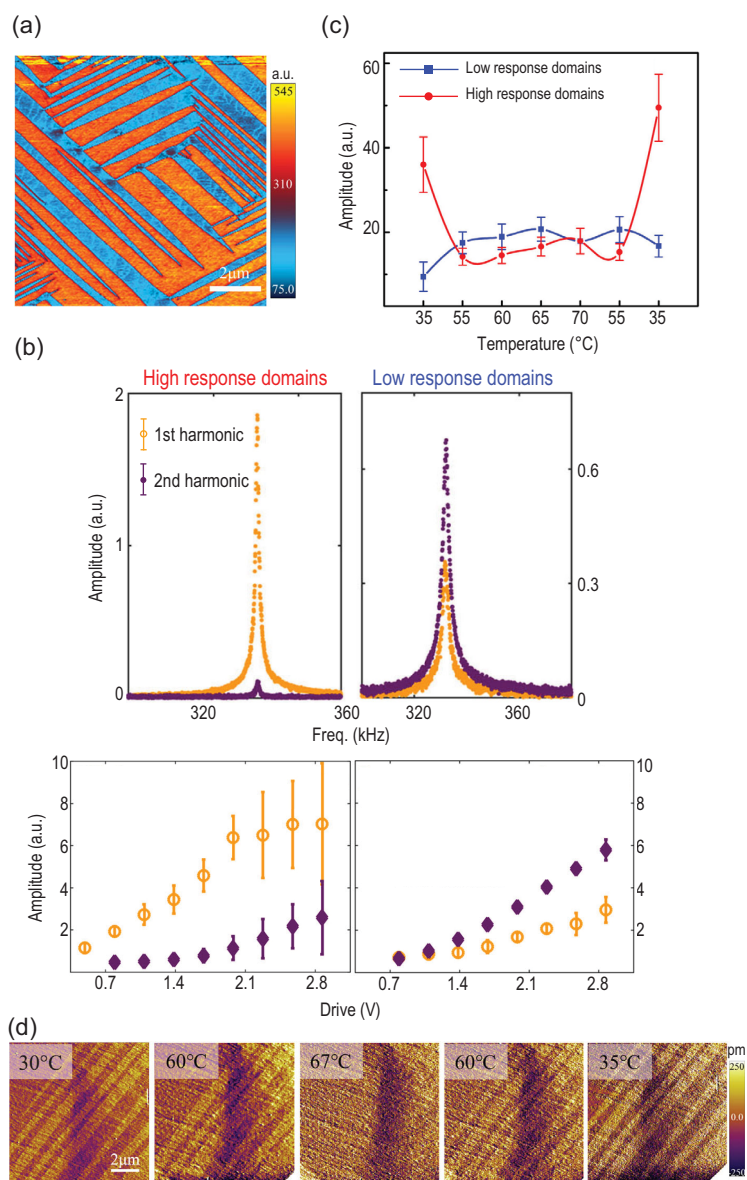


Figure 6. Alternating polar and nonpolar domains in MAPI. (a) Ferroic domain patterns of a MAPI crystal revealed by the vertical PFM. (b) The first row: point-wise tuning of piezoresponse versus frequency showing a point in high-response polar domain has dominant first harmonic response and negligible second harmonic one, while a point in low-response nonpolar domain has higher second harmonic response; the second row: comparison of first and second harmonic responses versus alternating current voltages averaged over a number of points in high- and low-response domains. (c) Piezoresponses averaged in high-response polar and low-response nonpolar domains showing opposite trend with respect to temperature, yet convergence beyond phase transition. (d) AFM topography mappings under a sequence of temperature across phase transition showing appearance and reemergence of ferroic domains. Adapted with permission from Ref. [4].

agreement on whether it is ferroelectric or not. The latest publication from Liu *et al.*, however, raised an alternative interpretation, that chemical and strain gradients induce flexoelectric polarization in MAPI [83]. This latest study seems to suggest symmetry

breaking in MAPI more aligned with polar structure, although its microscopic origin is different.

In 2018, we reported an in-depth PFM study [4] on single crystalline MAPI [84], with the goal to resolve the microscopic mechanisms of piezoresponse probed. We acquired the most compelling domain patterns (Fig. 6a), and established distinct mechanisms underlying the piezoresponse in adjacent domains (Fig. 6b) suggesting the coexistence of alternating polar and nonpolar structures. In particular, polar domains exhibit predominantly first harmonic linear response that arises from piezoelectricity, while nonpolar domains possess predominantly second harmonic quadratic response arising from ionic motion induced electrochemical dipoles [85]. This interpretation is supported by the drastically different thermal variation of piezoresponses in polar and nonpolar domains, one increasing with temperature, the other decreasing with temperature (Fig. 6c), which converge above cubic-tetragonal transition temperature. When the temperature is reduced, the original domain configuration is recovered (Fig. 6d), demonstrating a strong memory effect. In our view, this set of data unambiguously establishes alternating polar and nonpolar domains in our crystal, and this observation can reconcile all the inconsistent experimental data and theoretical analysis reported in the literature. Other PFM studies rarely examine the linear versus quadratic piezoresponses, and thus it is difficult to identify the dominant mechanisms critical for the differentiation. Theoretical calculation suggested that the energetic difference between polar and nonpolar lattice is tiny, <100 meV [9], and thus depending on composition, processing and environment, the balance can be easily tipped, making both structures possible in experiments. As summarized in Table 1, OIHPs with various compositions are reported to be either polar or nonpolar [5,6,12,19,39,41,42,44,45,47–60,62–68,73,76,83,86–101]. In addition, the processing methods may also affect the polarity of MAPI. A comparison of the representative preparation methods for MAPI reported to be polar [52–54,57] and nonpolar [60,68,102] presents that treating MAPI with dimethylformamide (DMF) vapor on a hotplate after general synthesis procedure and inclusion of methylammonium chloride (MACl) or PbCl_2 , in which chlorine was shown to be beneficial for obtaining MAPI with large grains [103], together with methylammonium iodide (MAI) during synthesis might be favorable for forming polar MAPI. In a sense, we all are both wrong and right that OIHPs can be both polar and nonpolar.

If MAPI is polar, can its polarity be switched? Macroscopically this is difficult to resolve, as the data are often smeared by leakage current, ionic

Table 1. Literature survey on the polarity of OIHPs with various compositions.

Composition	Non-polar	Polar
MAPbCl ₃	Refs [66,86]	Ref. [39]
MAPbBr ₃	Refs [19,66,87–89]	Refs [39,73,90]
MAPbI ₃	Refs [5,12,19,42,44,45,59,60,62,68,91]	Refs [6,41,47–58,76,83,92]
FAPbBr ₃		Ref. [94]
FAPbI ₃	Ref. [95]	Ref. [93]
CsPbCl ₃	Refs [96–98]	
CsPbBr ₃	Ref. [99]	Refs [100,101]
CsFAMAPbI _x Br _{3-x}	Ref. [63]	

migration as well as spatial averaging. Nevertheless, a number of recent reports indicate that electric field can indeed manipulate the domain structures [47,54,104], pointing toward a ferroelectric nature of the domain. The unambiguous switching of MAPI domains, however, requires further studies. We also note that ferroelectricity has been reported in MAPB [90], CsPbBr₃ [101] and mixed perovskites [93,105,106].

PHOTOVOLTAIC IMPLICATIONS

It is also important to examine the implications of OIHPs' polarity, or lack of it, to photovoltaic conversion, otherwise the problem remains largely academic. We have indeed observed photo-induced domain switching in MAPI via PFM [58], and a similar phenomenon has been observed under photo-excited scanning tunneling microscopy (STM) [107]. The light-domain interactions have been studied by Liu *et al.* [91,108], and poling has been shown to shift diode characteristic of MAPI [54]. Furthermore, piezoelectric modulations of photocurrent have also been observed [109,110]. All these studies suggest that polar structure may influence the photovoltaic conversion process, and to the very least, band bending induced by spontaneous polarization can either promote or hinder carrier transport, depending on its direction. Our study in 2018 indeed revealed that a polar domain possesses smaller photocurrent compared to a nonpolar one [4] (Fig. 7a), and upon heating and cooling across phase transition, a memory effect in photocurrent analogue to ferroic domains is also observed (Fig. 7b), confirming modulation of photocurrent by domains.

Nevertheless, there remains controversy about the effect of polarization on photovoltaic hysteresis. Unfavorable hysteresis is usually observed in the current-voltage ($I-V$) curve at various scanning rates or directions [111], casting doubts on the validity of the performance of solar cells and making it

hard to compare stability data among them. Despite booming research and significant progress on the efficiency of perovskite solar cells, fundamental understanding of frequently observed hysteresis is still inadequate.

Among various interpretations of hysteresis, ferroelectricity was suggested as one plausible origin at the very beginning. For example, Wei *et al.* attributed the hysteresis to the ferroelectric effect and built a ferroelectric diode model to explain the dependence of hysteresis on the scan range as well as the velocity [112]. They pointed out that special attention should be paid to optimization of power conversion efficiency. Recently, Ma *et al.* investigated correlations between the interfacial ferroelectricity and the hysteresis of specific heterojunctions by simulations [113]. They found that ferroelectricity is suppressed at the FAPbI₃/TiO₂ and MAPbI₃/phenyl-C61-butyric-acid-methyl-ester (PCBM) interfaces. The substitution of strong polar MA (dipole moment: 2.29 D) by weak polar FA ions (dipole moment: 0.29 D) and interface passivation could eliminate the interfacial electric field between perovskite and TiO₂, leading to consistent interfacial electronic dynamics and the absence of hysteresis [113]. Although it is now generally accepted that ions play a more important role in hysteresis [60,114,115], the separation of ionic effect and polar order is not trivial. For example, it has been reported that a dipolar Frenkel pair can be induced by ionic migration [116]. Meloni *et al.* claimed that hysteresis results from polarization of halide ion (vacancy) migration in the perovskite layer under the influence of the built-in and applied potential. The mobility of the other possible ionic species (MA⁺ and Pb²⁺) is much lower and not expected to give any significant contribution to polarization of devices [114]. We also found that while illumination may enhance polar response in Cs_{0.05}FA_{0.81}MA_{0.14}PbI_{2.55}Br_{0.45} (CsFAMA), only small photovoltaic hysteresis is observed at both the nano- and macroscale, demonstrating that the presence of strong polarization plays a negligible role in photovoltaic hysteresis. Based on multi-harmonic measurements, our study supports the concept that the primary mechanism responsible for photovoltaic hysteresis is ionic migration rather than polarization for this material [117].

CONCLUSION AND OUTLOOK

Theoretical calculation is a versatile tool to reveal the interaction of MA with the Pb-I framework, and study the influence of MA orientation on optoelectronic properties at the nanoscale. Adequate achievements have been reported and some

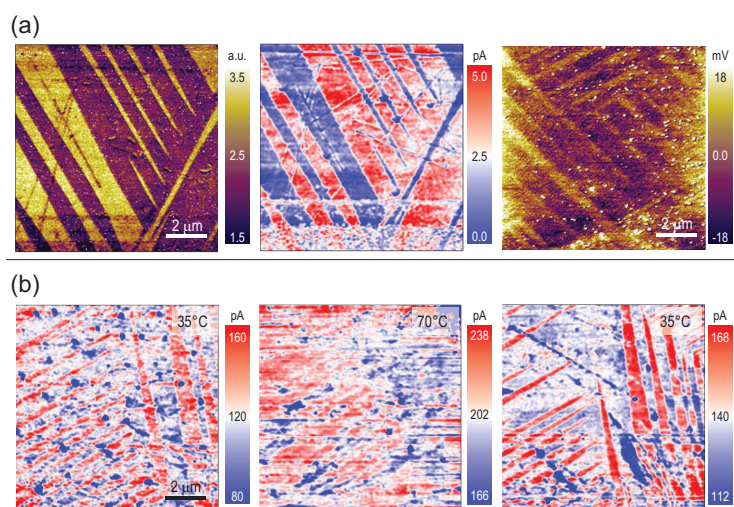


Figure 7. Regulation of photocurrent by polar domains. (a) Correlation between PFM (left) and photocurrent (middle) of the same area with reduced photocurrent in polar domains; and surface potential distribution under light follows ferroic domain pattern in Fig. 6a with negatively shifted potential in polar domains. (b) Photocurrent distribution in a separate domain pattern at different temperatures across phase transition, showing the disappearing domain pattern at 70°C upon heating and its reemergence at 35°C after cooling. Adapted with permission from Ref. [4].

common views have been reached: (i) the orientation of MA is determined by the hydrogen bond and usually faces towards the low-index direction; (ii) the orientation of MA can cause deformation of the Pb-I framework because of the H...I hydrogen bond, which can break the symmetry of the system and cause polarization; (iii) just tuning the orientation of MA, namely, polarization or not has little influence on the value of band gap, can cause direct-indirect band transition, as well as the Rashba/Dresselhaus effect or even dynamic Rashba/Dresselhaus effect, which may reduce the recombination of carrier, increase the carrier lifetime and enhance the optoelectronic performance.

Experimental observations on the ferroic properties of perovskite solar cells were systematically reviewed, along with photovoltaic implications: (i) a subtle difference between polar and nonpolar structure cannot be resolved by diffraction techniques, TEM, conventional macroscopic measurements and SHG in a conclusive way because of sample damage or an averaging effect; (ii) a powerful scanning probe can capture spatially resolved functional response from different structures, although caution must be exercised to distinguish complex microscopic mechanisms among polarity, ionic motion and defect; (iii) modulation of photocurrent by polar and nonpolar domains is confirmed, while ions may play a more important role in hysteresis, which is crucial for the performance of solar cells.

We may find that polarization, whatever its exact origins, plays only marginal roles in PSCs, but the endeavor often brings in unexpected twists. As shown in Fig. 8, giant electrostriction has been reported [116], which was attributed to defect dipoles of Frenkel pairs induced by ionic migration. Here, it seems impossible to distinctly separate ionic migration, defect and polarity, all of which will be reflected in the experimental observations.

Although the beam-induced damage of synchrotron diffraction and scanning transmission electron microscopy on perovskite samples is inevitable, with continuous improvement in characterization as well as material stability [118–121], it is hoped that these techniques will ultimately settle the debate as shown in Table 2, by resolving the structure details of OIHPs. For example, Breternitz *et al.* recently presented crystallographic evidence that the symmetry breaking on MAPI comes from interaction of polar cation MA with the anion framework via synchrotron diffraction [13]. Besides, tentative efforts have been made to mitigate the damage for acquiring atomically resolved imaging [118], including but not limited to using cryo-conditions for higher dose tolerance of sample [122], increasing acceleration voltage to decrease radiolysis [123], and taking advantage of facet-dependent electron beam sensitivity [119]. Although further investigation is required to examine their validity, these methods have provided promising directions for future characterizations. In addition, macroscopic techniques, such as impedance spectroscopy [124,125], in combination with modeling and simulation, may provide valuable supporting data on the microscopic mechanisms. In this regard, integrating a local scanning probe with global macroscopic measurements *in situ* will provide invaluable microscopic insight into the macroscopic phenomena, which we are trying to develop, and it is particularly important to examine different and often competing dynamical processes from local relaxation studies [126]. From a theoretical perspective, as the energy difference between the polar and nonpolar phases is tiny and might varies with different functionals or methods, calculations with higher accuracy should be performed. In parallel, a study on the polarization should proceed not only microscopically but also mesoscopically considering the long-range interaction of the ferroelectric domains. Therefore, *ab initio* calculations of the larger-scale system are also needed. To mimic the real experimental conditions, other factors including temperature, strain and light should also be taken into account to investigate the dynamics of OIHP. Combined with the machine learning and artificial intelligence algorithm [127], the classical molecular

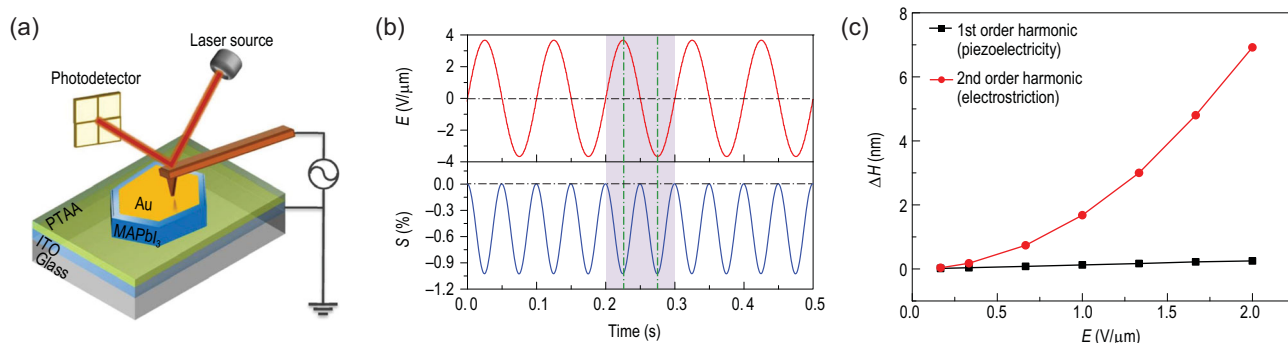


Figure 8. Electrostrictive response of MAPI single crystal. (a) Schematic illustration of AFM measurement of strain induced by electric field. (b) Electrostrictive strain of a 40 μm MAPI single crystal under a.c. bias at 10 Hz. (c) Thickness change measured by Mach-Zehnder interferometer resulting from first-order piezoelectricity and second-order electrostriction for a 40 μm MAPI single crystal under 100 Hz a.c. with different field amplitudes. Adapted with permission from Ref. [116].

Table 2. Literature survey on the polarity of OIHPs.

Technique	Nonpolar I4/mcm	Polar I4cm	Noncommittal
X-ray and neutron diffractions	Refs [5,42–45]	Refs [6,41]	Ref. [40]
Optic SHG	Refs [12,19,62,67]	Refs [76,93]	
Macroscopic measurements	Refs [59,60,64]	Refs [48,50,76,90,101]	Ref. [75]
Microscopic PFM	Refs [8,63,65,68,91]	Refs [46,47,49–58,83]	Refs [61,80,81,104]
TEM		Ref. [73]	Ref. [70]
DFT and MD simulations	Refs [12,19,66]	Ref. [92]	Refs [8,21]

dynamic simulation with accurate potential energy surface also needs to be improved. So are OIHPs polar or nonpolar? That might not be the question, but efforts made to answer it continue to deliver new insights.

ACKNOWLEDGEMENTS

We acknowledge the support of the Center for Computational Science and Engineering at Southern University of Science and Technology.

FUNDING

This work was supported by the Key-Area Research and Development Program of Guangdong Province (2018B010109009), the Shenzhen Science and Technology Innovation Committee (JCYJ20180507182257563), the National Natural Science Foundation of China (11772207 and 22003074), the Instrument Developing Project of Chinese Academy of Sciences (ZDKYYQ20180004), the Natural Science Foundation of Guangdong Province (2017A030313342 and 2020A1515110580), the State Key Laboratory of Mechanics and Control of Mechanical Structures (Nanjing University of Aeronautics and Astronautics) (MCMS-E-0420G01), the Guangdong Provincial Key Laboratory Program from the Department of Science and Technology of Guangdong Province (2021B1212040001), and the SIAT Innovation Program for Excellent Young Researchers.

Conflict of interest statement. None declared.

REFERENCES

- Frost JM, Butler KT and Brivio F *et al.* Atomistic origins of high-performance in hybrid halide perovskite solar cells. *Nano Lett* 2014; **14**: 2584–90.
- Liu Y, Collins L and Proksch R *et al.* Reply to: on the ferroelectricity of $\text{CH}_3\text{NH}_3\text{PbI}_3$ perovskites. *Nat Mater* 2019; **18**: 1051–3.
- Schulz AD, Röhm H and Leonhard T *et al.* On the ferroelectricity of $\text{CH}_3\text{NH}_3\text{PbI}_3$ perovskites. *Nat Mater* 2019; **18**: 1050.
- Huang B, Kong G and Esfahani EN *et al.* Ferroic domains regulate photocurrent in single-crystalline $\text{CH}_3\text{NH}_3\text{PbI}_3$ films self-grown on FTO/ TiO_2 substrate. *npj Quant Mater* 2018; **3**: 30.
- Baikie T, Fang Y and Kadro JM *et al.* Synthesis and crystal chemistry of the hybrid perovskite $(\text{CH}_3\text{NH}_3)\text{PbI}_3$ for solid-state sensitised solar cell applications. *J Mater Chem A* 2013; **1**: 5628–41.
- Stoumpos CC, Malliakas CD and Kanatzidis MG. Semiconducting tin and lead iodide perovskites with organic cations: phase transitions, high mobilities, and near-infrared photoluminescent properties. *Inorg Chem* 2013; **52**: 9019–38.
- Yin WJ, Yang JH and Kang J *et al.* Halide perovskite materials for solar cells: a theoretical review. *J Mater Chem A* 2015; **3**: 8926–42.

8. Fan Z, Xiao J and Sun K *et al.* Ferroelectricity of $\text{CH}_3\text{NH}_3\text{PbI}_3$ perovskite. *J Phys Chem Lett* 2015; **6**: 1155–61.
9. Quarti C, Mosconi E and De Angelis F. Interplay of orientational order and electronic structure in methylammonium lead iodide: implications for solar cell operation. *Chem Mater* 2014; **26**: 6557–69.
10. Stroppa A, Quarti C and De Angelis F *et al.* Ferroelectric polarization of $\text{CH}_3\text{NH}_3\text{PbI}_3$: a detailed study based on density functional theory and symmetry mode analysis. *J Phys Chem Lett* 2015; **6**: 2223–31.
11. Zheng F, Takenaka H and Wang F *et al.* First-principles calculation of the bulk photovoltaic effect in $\text{CH}_3\text{NH}_3\text{PbI}_3$ and $\text{CH}_3\text{NH}_3\text{PbI}_{3-x}\text{Cl}_x$. *J Phys Chem Lett* 2015; **6**: 31–7.
12. Frohna K, Deshpande T and Harter J *et al.* Inversion symmetry and bulk Rashba effect in methylammonium lead iodide perovskite single crystals. *Nat Commun* 2018; **9**: 1829.
13. Breternitz J, Lehmann F and Barnett SA *et al.* Role of the iodide-methylammonium interaction in the ferroelectricity of $\text{CH}_3\text{NH}_3\text{PbI}_3$. *Angew Chem Int Ed* 2020; **59**: 424–8.
14. Brivio F, Walker AB and Walsh A. Structural and electronic properties of hybrid perovskites for high-efficiency thin-film photovoltaics from first-principles. *APL Mater* 2013; **1**: 042111.
15. Bechtel JS, Seshadri R and Van der Ven A. Energy landscape of molecular motion in cubic methylammonium lead iodide from first-principles. *J Phys Chem C* 2016; **120**: 12403–10.
16. Shimamura K, Hakamata T and Shimojo F *et al.* Rotation mechanism of methylammonium molecules in organometal halide perovskite in cubic phase: an ab initio molecular dynamics study. *J Chem Phys* 2016; **145**: 224503.
17. Xu Q, Stroppa A and Lv J *et al.* Impact of organic molecule rotation on the optoelectronic properties of hybrid halide perovskites. *Phys Rev Mater* 2019; **3**: 125401.
18. Svane KL, Forse AC and Grey CP *et al.* How strong is the hydrogen bond in hybrid perovskites? *J Phys Chem Lett* 2017; **8**: 6154–9.
19. Govinda S, Kore BP and Bokdam M *et al.* Behavior of methylammonium dipoles in MAPbX_3 ($X = \text{Br}$ and I). *J Phys Chem Lett* 2017; **8**: 4113–21.
20. Li Y, Behtash M and Wong J *et al.* Enhancing ferroelectric dipole ordering in organic-inorganic hybrid perovskite $\text{CH}_3\text{NH}_3\text{PbI}_3$: strain and doping engineering. *J Phys Chem C* 2018; **122**: 177–84.
21. Mattoni A, Filippetti A and Saba M *et al.* Methylammonium rotational dynamics in lead halide perovskite by classical molecular dynamics: the role of temperature. *J Phys Chem C* 2015; **119**: 17421–8.
22. Mosconi E, Quarti C and Ivanovska T *et al.* Structural and electronic properties of organo-halide lead perovskites: a combined IR-spectroscopy and ab initio molecular dynamics investigation. *Phys Chem Chem Phys* 2014; **16**: 16137–44.
23. Carignano MA, Kachmar A and Hutter J. Thermal effects on $\text{CH}_3\text{NH}_3\text{PbI}_3$ perovskite from ab initio molecular dynamics simulations. *J Phys Chem C* 2015; **119**: 8991–7.
24. Long R, Fang W and Prezhdo OV. Moderate humidity delays electron-hole recombination in hybrid organic-inorganic perovskites: time-domain ab initio simulations rationalize experiments. *J Phys Chem Lett* 2016; **7**: 3215–22.
25. Geng W, Hu Q and Tong CJ *et al.* The Influence of dipole moments induced by organic molecules and domain structures on the properties of $\text{CH}_3\text{NH}_3\text{PbI}_3$ perovskite. *Adv Theory Simul* 2019; **2**: 1900041.
26. Mladenović M and Vukmirović N. Effects of thermal disorder on the electronic structure of halide perovskites: insights from MD simulations. *Phys Chem Chem Phys* 2018; **20**: 25693–700.
27. Motta C, El-Mellouhi F and Kais S *et al.* Revealing the role of organic cations in hybrid halide perovskite $\text{CH}_3\text{NH}_3\text{PbI}_3$. *Nat Commun* 2015; **6**: 7026.
28. Motta C, El-Mellouhi F and Sanvito S. Exploring the cation dynamics in lead-bromide hybrid perovskites. *Phys Rev B* 2016; **93**: 235412.
29. Leppert L, Reyes-Lillo SE and Neaton JB. Electric field- and strain-induced Rashba effect in hybrid halide perovskites. *J Phys Chem Lett* 2016; **7**: 3683–9.
30. Niesner D, Wilhelm M and Levchuk I *et al.* Giant Rashba splitting in $\text{CH}_3\text{NH}_3\text{PbBr}_3$ organic-inorganic perovskite. *Phys Rev Lett* 2016; **117**: 126401.
31. Etienne T, Mosconi E and De Angelis F. Dynamical origin of the Rashba effect in organohalide lead perovskites: a key to suppressed carrier recombination in perovskite solar cells? *J Phys Chem Lett* 2016; **7**: 1638–45.
32. Zheng F, Tan LZ and Liu S *et al.* Rashba spin-orbit coupling enhanced carrier lifetime in $\text{CH}_3\text{NH}_3\text{PbI}_3$. *Nano Lett* 2015; **15**: 7794–800.
33. Niesner D, Hauck M and Shrestha S *et al.* Structural fluctuations cause spin-split states in tetragonal $(\text{CH}_3\text{NH}_3)\text{PbI}_3$ as evidenced by the circular photogalvanic effect. *Proc Natl Acad Sci USA* 2018; **115**: 9509–14.
34. Wu B, Yuan HF and Xu Q *et al.* Indirect tail states formation by thermal-induced polar fluctuations in halide perovskites. *Nat Commun* 2019; **10**: 484.
35. Kepenekian M, Robles R and Katan C *et al.* Rashba and Dresselhaus effects in hybrid organic-inorganic perovskites: from basics to devices. *ACS Nano* 2015; **9**: 11557–67.
36. Chen L, Paillard C and Zhao HJ *et al.* Tailoring properties of hybrid perovskites by domain-width engineering with charged walls. *NPJ Comput Mater* 2018; **4**: 75.
37. Ma J and Wang L-W. Nanoscale charge localization induced by random orientations of organic molecules in hybrid perovskite $\text{CH}_3\text{NH}_3\text{PbI}_3$. *Nano Lett* 2015; **15**: 248–53.
38. Qiao L, Fang W-H and Long R. Ferroelectric polarization suppresses nonradiative electron-hole recombination in $\text{CH}_3\text{NH}_3\text{PbI}_3$ perovskites: a time-domain ab initio study. *J Phys Chem Lett* 2019; **10**: 7237–44.
39. Liu S, Zheng F and Koocher NZ *et al.* Ferroelectric domain wall induced band gap reduction and charge separation in organometal halide perovskites. *J Phys Chem Lett* 2015; **6**: 693–9.
40. Baikie T, Barrow NS and Fang YA *et al.* A combined single crystal neutron/X-ray diffraction and solid-state nuclear magnetic resonance study of the hybrid perovskites $\text{CH}_3\text{NH}_3\text{PbX}_3$ ($X = \text{I}, \text{Br}$ and Cl). *J Mater Chem A* 2015; **3**: 9298–307.
41. Dang YY, Liu Y and Sun YX *et al.* Bulk crystal growth of hybrid perovskite material $\text{CH}_3\text{NH}_3\text{PbI}_3$. *CrystEngComm* 2015; **17**: 665–70.
42. Fang HH, Raissa R and Abdu-Aguye M *et al.* Photophysics of organic-inorganic hybrid lead iodide perovskite single crystals. *Adv Funct Mater* 2015; **25**: 2378–85.
43. Sewwandi GA, Kodera K and Ma H *et al.* Antiferroelectric nature of $\text{CH}_3\text{NH}_3\text{PbI}_{3-x}\text{Cl}_x$ perovskite and its implication for charge separation in perovskite solar cells. *Sci Rep* 2016; **6**: 30680.
44. Weller MT, Weber OJ and Henry PF *et al.* Complete structure and cation orientation in the perovskite photovoltaic methylammonium lead iodide between 100 and 352 K. *Chem Commun* 2015; **51**: 4180–3.
45. Whitfield PS, Herron N and Guise WE *et al.* Structures, phase transitions and tricritical behavior of the hybrid perovskite methyl ammonium lead iodide. *Sci Rep* 2016; **6**: 35685.
46. Chen B, Shi J and Zheng X *et al.* Ferroelectric solar cells based on inorganic-organic hybrid perovskites. *J Mater Chem A* 2015; **3**: 7699–705.
47. Garten LM, Moore DT and Nanayakkara SU *et al.* The existence and impact of persistent ferroelectric domains in MAPbI_3 . *Sci Adv* 2019; **5**: eaas9311.

48. Guo H, Liu P and Zheng S *et al.* Re-entrant relaxor ferroelectricity of methylammonium lead iodide. *Curr Appl Phys* 2016; **16**: 1603–6.
49. Kim H-S, Kim SK and Kim BJ *et al.* Ferroelectric polarization in $\text{CH}_3\text{NH}_3\text{PbI}_3$ perovskite. *J Phys Chem Lett* 2015; **6**: 1729–35.
50. Kim Y-J, Dang T-V and Choi H-J *et al.* Piezoelectric properties of $\text{CH}_3\text{NH}_3\text{PbI}_3$ perovskite thin films and their applications in piezoelectric generators. *J Mater Chem A* 2016; **4**: 756–63.
51. Kutes Y, Ye L and Zhou Y *et al.* Direct observation of ferroelectric domains in solution-processed $\text{CH}_3\text{NH}_3\text{PbI}_3$ perovskite thin films. *J Phys Chem Lett* 2014; **5**: 3335–9.
52. Leonhard T, Schulz AD and Röhm H *et al.* Probing the microstructure of methylammonium lead iodide perovskite solar cells. *Energy Technol.* 2019; **7**: 1800989.
53. Röhm H, Leonhard T and Hoffmann M *et al.* Ferroelectric domains in methylammonium lead iodide perovskite thin-films. *Energy Environ Sci* 2017; **10**: 950–5.
54. Röhm H, Leonhard T and Hoffmann MJ *et al.* Ferroelectric poling of methylammonium lead iodide thin films. *Adv Funct Mater* 2020; **30**: 1908657.
55. Rohm H, Leonhard T and Schulz AD *et al.* Ferroelectric properties of perovskite thin films and their implications for solar energy conversion. *Adv Mater* 2019; **31**: 1806661.
56. Seol D, Jeong A and Han MH *et al.* Origin of hysteresis in $\text{CH}_3\text{NH}_3\text{PbI}_3$ perovskite thin films. *Adv Funct Mater* 2017; **27**: 1701924.
57. Vorpahl SM, Giridharagopal R and Eperon GE *et al.* Orientation of ferroelectric domains and disappearance upon heating methylammonium lead triiodide perovskite from tetragonal to cubic phase. *ACS Appl Energy Mater* 2018; **1**: 1534–9.
58. Wang P, Zhao J and Wei L *et al.* Photo-induced ferroelectric switching in perovskite $\text{CH}_3\text{NH}_3\text{PbI}_3$ films. *Nanoscale* 2017; **9**: 3806–17.
59. Anusca I, Balčiūnas S and Gemeiner P *et al.* Dielectric response: answer to many questions in the methylammonium lead halide solar cell absorbers. *Adv Energy Mater* 2017; **7**: 1700600.
60. Beilstein-Edmands J, Eperon G and Johnson R *et al.* Non-ferroelectric nature of the conductance hysteresis in $\text{CH}_3\text{NH}_3\text{PbI}_3$ perovskite-based photovoltaic devices. *Appl Phys Lett* 2015; **106**: 173502.
61. Coll M, Gomez AS and Mas-Marza E *et al.* Polarization switching and light-enhanced piezoelectricity in lead halide perovskites. *J Phys Chem Lett* 2015; **6**: 1408–13.
62. Govinda S, Mahale P and Kore BP *et al.* Is $\text{CH}_3\text{NH}_3\text{PbI}_3$ polar? *J Phys Chem Lett* 2016; **7**: 2412–9.
63. Gómez A, Wang Q and Goñi AR *et al.* Ferroelectricity-free lead halide perovskites. *Energy Environ Sci* 2019; **12**: 2537–47.
64. Hoque MNF, Yang M and Li Z *et al.* Polarization and dielectric study of methylammonium lead iodide thin film to reveal its nonferroelectric nature under solar cell operating conditions. *ACS Energy Lett* 2016; **1**: 142–9.
65. Liu Y, Collins L and Belianinov A *et al.* Dynamic behavior of $\text{CH}_3\text{NH}_3\text{PbI}_3$ perovskite twin domains. *Appl Phys Lett* 2018; **113**: 072102.
66. Šimėnas M, Balčiūnas S and Maćzka M *et al.* Exploring the antipolar nature of methylammonium lead halides: a Monte Carlo and pyrocurrent study. *J Phys Chem Lett* 2017; **8**: 4906–11.
67. Yamada Y, Yamada T and Phuonng LQ *et al.* Dynamic optical properties of $\text{CH}_3\text{NH}_3\text{PbI}_3$ single crystals as revealed by one- and two-photon excited photoluminescence measurements. *J Am Chem Soc* 2015; **137**: 10456–9.
68. Liu Y, Collins L and Proksch R *et al.* Chemical nature of ferroelastic twin domains in $\text{CH}_3\text{NH}_3\text{PbI}_3$ perovskite. *Nat Mater* 2018; **17**: 1013–9.
69. Chen S, Zhang X and Zhao J *et al.* Atomic scale insights into structure instability and decomposition pathway of methylammonium lead iodide perovskite. *Nat Commun* 2018; **9**: 4807.
70. Rothmann MU, Li W and Zhu Y *et al.* Direct observation of intrinsic twin domains in tetragonal $\text{CH}_3\text{NH}_3\text{PbI}_3$. *Nat Commun* 2017; **8**: 14547.
71. Rothmann MU, Li W and Zhu Y *et al.* Structural and chemical changes to $\text{CH}_3\text{NH}_3\text{PbI}_3$ induced by electron and gallium ion beams. *Adv Mater* 2018; **30**: 1800629.
72. Saliba M, Stolterfoht M and Wolff CM *et al.* Measuring aging stability of perovskite solar cells. *Joule* 2018; **2**: 1019–24.
73. Zhang D, Zhu Y and Liu L *et al.* Atomic-resolution transmission electron microscopy of electron beam-sensitive crystalline materials. *Science* 2018; **359**: 675–9.
74. Birkhold ST, Hu H and Höger PT *et al.* Mechanism and impact of cation polarization in methylammonium lead iodide. *J Phys Chem C* 2018; **122**: 12140–7.
75. Cordero F, Craciun F and Trequattrini F *et al.* Competition between polar and antiferrodistortive modes and correlated dynamics of the methylammonium molecules in MAPbI_3 from anelastic and dielectric measurements. *J Phys Chem Lett* 2018; **9**: 4401–6.
76. Rakita Y, Bar-Elli O and Meirzadeh E *et al.* Tetragonal $\text{CH}_3\text{NH}_3\text{PbI}_3$ is ferroelectric. *Proc Natl Acad Sci USA* 2017; **114**: E5504–12.
77. Govinda S, Kore BP and Mahale P *et al.* Can SHG measurements determine the polarity of hybrid lead halide perovskites? *ACS Energy Lett* 2018; **3**: 1887–91.
78. Bonnell DA, Kalinin SV and Kholkin A *et al.* Piezoresponse force microscopy: a window into electromechanical behavior at the nanoscale. *MRS Bull* 2009; **34**: 648–57.
79. Li J, Li J-F and Yu Q *et al.* Strain-based scanning probe microscopies for functional materials, biological structures, and electrochemical systems. *J Materomics* 2015; **1**: 3–21.
80. Hermes IM, Bretschneider SA and Bergmann VW *et al.* Ferroelastic fingerprints in methylammonium lead iodide perovskite. *J Phys Chem C* 2016; **120**: 5724–31.
81. Strelcov E, Dong Q and Li T *et al.* $\text{CH}_3\text{NH}_3\text{PbI}_3$ perovskites: ferroelasticity revealed. *Sci Adv* 2017; **3**: e1602165.
82. Chen QN, Ou Y and Ma F *et al.* Mechanisms of electromechanical coupling in strain based scanning probe microscopy. *Appl Phys Lett* 2014; **104**: 242907.
83. Liu Y, Ilev AV and Collins L *et al.* Strain-chemical gradient and polarization in metal halide perovskites. *Adv Electron Mater* 2020; **6**: 1901235.
84. Zhao J, Kong G and Chen S *et al.* Single crystalline $\text{CH}_3\text{NH}_3\text{PbI}_3$ self-grown on FTO/ TiO_2 substrate for high efficiency perovskite solar cells. *Sci Bull* 2017; **62**: 1173–6.
85. Yu J, Esfahani EN and Zhu Q *et al.* Quadratic electromechanical strain in silicon investigated by scanning probe microscopy. *J Appl Phys* 2018; **123**: 155104.
86. Bari M, Bokov AA and Ye ZG. Ferroelasticity, domain structures and phase symmetries in organic-inorganic hybrid perovskite methylammonium lead chloride. *J Mater Chem C* 2020; **8**: 9625–31.
87. Gonzalez-Carrero S, Frances-Soriano L and Gonzalez-Bejar M *et al.* The luminescence of $\text{CH}_3\text{NH}_3\text{PbBr}_3$ perovskite nanoparticles crests the summit and their photostability under wet conditions is enhanced. *Small* 2016; **12**: 5245–50.
88. Mashiyama H, Kawamura Y and Kubota Y. The anti-polar structure of $\text{CH}_3\text{NH}_3\text{PbBr}_3$. *J Korean Phys Soc* 2007; **51**: 850–3.
89. Bari M, Bokov AA and Ye Z-G. Ferroelastic domains and phase transitions in organic-inorganic hybrid perovskite $\text{CH}_3\text{NH}_3\text{PbBr}_3$. *J Mater Chem C* 2021; **9**: 3096–107.

90. Gao Z-R, Sun X-F and Wu Y-Y *et al.* Ferroelectricity of the orthorhombic and tetragonal MAPbBr₃ single crystal. *J Phys Chem Lett* 2019; **10**: 2522–7.
91. Liu Y, Levlev AV and Collins L *et al.* Light-ferroic interaction in hybrid organic-inorganic perovskites. *Adv Optical Mater* 2019; **7**: 1901451.
92. Frost JM, Butler KT and Walsh A. Molecular ferroelectric contributions to anomalous hysteresis in hybrid perovskite solar cells. *APL Mater* 2014; **2**: 081506.
93. Ahmadi M, Collins L and Poretzky A *et al.* Exploring anomalous polarization dynamics in organometallic halide perovskites. *Adv Mater* 2018; **30**: 1705298.
94. Ding R, Liu H and Zhang XL *et al.* Flexible piezoelectric nanocomposite generators based on formamidineum lead halide perovskite nanoparticles. *Adv Funct Mater* 2016; **26**: 7708–16.
95. Taylor VCA, Tiwari D and Duchi M *et al.* Investigating the role of the organic cation in formamidineum lead iodide perovskite using ultrafast spectroscopy. *J Phys Chem Lett* 2018; **9**: 895–901.
96. Voloshinovskii A, Myagkota S and Levitskii R. Luminescence of ferroelastic CsPbCl₃ nanocrystals. *Ferroelectrics* 2005; **317**: 311–5.
97. Lim AR and Jeong S-Y. Ferroelastic phase transition and twin structure by ¹³³Cs NMR in a CsPbCl₃ single crystal. *Physica B Condens Matter* 2001; **304**: 79–85.
98. Hirotsu S. Experimental studies of structural phase transitions in CsPbCl₃. *J Phys Soc Jpn* 1971; **31**: 552–60.
99. Marçal LA, Oksenberg E and Dzhibaev D *et al.* *In situ* imaging of ferroelastic domain dynamics in CsPbBr₃ perovskite nanowires by nanofocused scanning X-ray diffraction. *ACS Nano* 2020; **14**: 15973–82.
100. Zhao Y-Q, Ma Q-R and Liu B *et al.* Pressure-induced strong ferroelectric polarization in tetra-phase perovskite CsPbBr₃. *Phys Chem Chem Phys* 2018; **20**: 14718–24.
101. Li X, Chen S and Liu P-F *et al.* Evidence for ferroelectricity of all-inorganic perovskite CsPbBr₃ quantum dots. *J Am Chem Soc* 2020; **142**: 3316–20.
102. Chen Q, Zhou HP and Hong ZR *et al.* Planar heterojunction perovskite solar cells via vapor-assisted solution process. *J Am Chem Soc* 2014; **136**: 622–5.
103. Luo SQ and Daoud WA. Crystal structure formation of CH₃NH₃Pb_{1-x}Cl_x perovskite. *Materials* 2016; **9**: 123.
104. Kim D, Yun JS and Sharma P *et al.* Light- and bias-induced structural variations in metal halide perovskites. *Nat Commun* 2019; **10**: 444.
105. Xiao J, Chang J and Li B *et al.* Room temperature ferroelectricity of hybrid organic-inorganic perovskites with mixed iodine and bromine. *J Mater Chem A* 2018; **6**: 9665–76.
106. Zhang Q, Solanki A and Parida K *et al.* Tunable ferroelectricity in Ruddlesden-Popper halide perovskites. *ACS Appl Mater Interfaces* 2019; **11**: 13523–32.
107. Hsu H-C, Huang B-C and Chin S-C *et al.* Photodriven dipole reordering: key to carrier separation in metalorganic halide perovskites. *ACS Nano* 2019; **13**: 4402–9.
108. Liu Y, Li M and Wang M *et al.* Twin domains modulate light-matter interactions in metal halide perovskites. *APL Mater* 2020; **8**: 011106.
109. Khorramshahi F, Woughter AG and Ram MK *et al.* Apparent piezophotocurrent modulation in methylammonium lead iodide perovskite photodetectors. *Adv Electron Mater* 2019; **5**: 1900518.
110. Lai Q, Zhu L and Pang Y *et al.* Piezo-phototronic effect enhanced photodetector based on CH₃NH₃PbI₃ single crystals. *ACS Nano* 2018; **12**: 10501–8.
111. Ravishankar S, Gharibzadeh S and Roldan-Carmona C *et al.* Influence of charge transport layers on open-circuit voltage and hysteresis in perovskite solar cells. *Joule* 2018; **2**: 788–98.
112. Wei J, Zhao Y and Li H *et al.* Hysteresis analysis based on the ferroelectric effect in hybrid perovskite solar cells. *J Phys Chem Lett* 2014; **5**: 3937–45.
113. Ma W, Zhang X and Xu Z *et al.* Reducing anomalous hysteresis in perovskite solar cells by suppressing the interfacial ferroelectric order. *ACS Appl Mater Interfaces* 2020; **12**: 12275–84.
114. Meloni S, Moehl T and Tress W *et al.* Ionic polarization-induced current-voltage hysteresis in CH₃NH₃PbX₃ perovskite solar cells. *Nat Commun* 2016; **7**: 10334.
115. Shi JJ, Li YM and Li YS *et al.* From ultrafast to ultraslow: charge-carrier dynamics of perovskite solar cells. *Joule* 2018; **2**: 879–901.
116. Chen B, Li T and Dong Q *et al.* Large electrostrictive response in lead halide perovskites. *Nat Mater* 2018; **17**: 1020–6.
117. Xia G, Huang B and Zhang Y *et al.* Nanoscale insights into photovoltaic hysteresis in triple-cation mixed-halide perovskite: resolving the role of polarization and ionic migration. *Adv Mater* 2019; **31**: 1902870.
118. Chen S and Gao P. Challenges, myths, and opportunities of electron microscopy on halide perovskites. *J Appl Phys* 2020; **128**: 010901.
119. Chen S, Zhang Y and Zhao J *et al.* Transmission electron microscopy of organic-inorganic hybrid perovskites: myths and truths. *Sci Bull* 2020; **65**: 1643–9.
120. Ono LK, Qi YB and Liu SZ. Progress toward stable lead halide perovskite solar cells. *Joule* 2018; **2**: 1961–90.
121. Zhou YY, Sternlicht H and Padture NP. Transmission electron microscopy of halide perovskite materials and devices. *Joule* 2019; **3**: 641–61.
122. Li Y, Zhou W and Li Y *et al.* Unravelling degradation mechanisms and atomic structure of organic-inorganic halide perovskites by cryo-EM. *Joule* 2019; **3**: 2854–66.
123. Dang Z, Shamsi J and Palazon F *et al.* *In situ* transmission electron microscopy study of electron beam-induced transformations in colloidal cesium lead halide perovskite nanocrystals. *ACS Nano* 2017; **11**: 2124–32.
124. Jeong S-H, Park J and Han T-H *et al.* Characterizing the efficiency of perovskite solar cells and light-emitting diodes. *Joule* 2020; **4**: 1206–35.
125. Pitarch-Tena D, Ngo TT and Vallés-Pelarda M *et al.* Impedance spectroscopy measurements in perovskite solar cells: device stability and noise reduction. *ACS Energy Lett* 2018; **3**: 1044–8.
126. Yu JX, Huang BY and Li AL *et al.* Resolving local dynamics of dual ions at the nanoscale in electrochemically active materials. *Nano Energy* 2019; **66**: 104160.
127. Correa-Baena JP, Hippalgaonkar K and van Duren J *et al.* Accelerating materials development via automation, machine learning, and high-performance computing. *Joule* 2018; **2**: 1410–20.